the position of shock X_{s0} at zero turbulence level. The boundary-layer momentum thickness Reynolds number R_θ and boundary-layer displacement thickness δ^* measured just before the shock are also shown in the figure. It is observed that an increase in Tu from 0.3 to 6% produces a shift in the shock position of 20%. Such a large change in the shock position cannot be explained solely in terms of the thickening of the boundary layer associated with the increase in freestream turbulence. First, the initial increase in δ^* followed by a decrease is not likely to produce such a large shift in the shock position in one direction. This is shown by the experiments performed by Delery[3] on a similar model and at a constant freestream turbulence level. Second, R_θ does not increase continuously with the increase in Tu_∞, whereas the shock position shifts in only one direction with the increase in Tu_∞. Typically, Tu_∞ levels of 2.5 and 5.1% produce the same value of R_θ, whereas the shock positions for these two values of R_θ are not the same. It appears that the freestream turbulence has a direct effect on the shock interactions and, therefore, the shock position.

Figure 3 shows the influence of Tu on the peak Mach number on the model M_{pk}. The influence of Tu_∞ on M_{pk} is larger at $M_{pk} \gtrsim 1.3$, a condition corresponding to significant shock-induced separation. This suggests that the freestream turbulence plays an important part in strong adverse pressure gradients where large regions of separation are present.

The pressure distributions in the region of shock-induced separation for a constant value of $M_{pk} = 1.44$ and for various freestream turbulence levels Tu are shown in Fig. 4. The differences in C_p levels at the shock position are due to the differences in the freestream Mach numbers needed to achieve a constant value of M_{pk}. The shock position at this value of M_{pk} is typically 80% chord. Increase in Tu_∞ is shown to produce an increase in pressure recovery at the trailing edge of the model. Similar trends in C_p have been observed with the introduction of vortex generators.[4] The increase in pressure recovery is due to the increase in momentum transport from the freestream into the separated region produced by the turbulence.

China clay flow visualization showed a two-dimensional separation over 90% of the model span. Figure 5 shows the variation of separation length, nondimensionalized with respect to the boundary-layer thickness measured upstream of the shock, with the Reynolds number based on the boundary-layer thickness. When compared with the results of Kooi[5] it is seen that for given boundary-layer conditions upstream of the shock wave, the separation length is influenced by the freestream turbulence.

Thus it can be concluded that the freestream turbulence plays an important part in transonic flow with shock interactions. Detailed measurements of flowfield at various levels of the freestream turbulence are in progress.

References

[1] Green, J.E., "On the Influence of Free Stream Turbulence on a Turbulent Boundary Layer as it Relates to Wind Tunnel Testing at Subsonic Speeds," AGARD Report 602, 1973 and RAE TR 72201, 1972.

[2] Raghunathan, S. and McAdam, R.J.W., "Free Stream Turbulence and Attached Subsonic Turbulent Boundary Layer," AIAA Paper 82-0029, Jan. 1982.

[3] Delery, J., "Some Features of Transonic Shock Wave Turbulent Boundary Layer Interaction," *Shock Boundary Layer Interactions in Turbomachines,* Von Kármán Institute Lecture Series, Brussels, No. 8, 1980, pp. 1-17.

[4] Green, J.E., "Interactions between Shock Waves and Turbulent Boundary Layers," RAE TR 69098, May 1969.

[5] Kooi, J.W., "Influence of Free Stream Mach Number on Transonic Shock Wave Boundary Layer Interaction," NLR MP 78013u, 1978.

Dynamic Stability Boundaries for a Sinusoidal Shallow Arch under Pulse Loads

Michael T. Donaldson* and Raymond H. Plaut†
Virginia Polytechnic Institute and State University, Blacksburg, Virginia

Introduction

THE dynamic snap-through of a shallow elastic arch subjected to triangular pulse loads is investigated. Concentrated loads with independent magnitudes are applied at the quarter points of the arch as a means of assessing the effects of load asymmetry. Critical load combinations are determined and the effects of the pulse duration and external damping on the interaction curves are examined. The behavior is similar to that of some shallow shells under blast loads and demonstrates that asymmetric loading may have much lower critical values than symmetric loading.

Humphreys[1] and Fulton and Barton[2] investigated the instability of arches subjected to rectangular pulse loads. External damping was considered by Lock[3] and Hegemier and Tzung,[4] whereas Huang and Nachbar[5] and Johnson[6] treated material damping with a Kelvin-Voigt model. Step loads were applied in Refs. 3-5 and impulse loads in Ref. 6. Interaction curves for multiple step loads were presented by Gregory and Plaut.[7]

Analysis

The ends of the arch are simply supported, the unloaded configuration is

$$Y_0(X) = \Lambda \sin(\pi X/L) \qquad 0 \le X \le L \tag{1}$$

and the shape at time T is $Y(X,T)$. The arch has mass μ per unit length, Young's modulus E, cross-sectional area A, moment of inertia I, and radius of gyration $r = \sqrt{I/A}$. Concentrated downward loads $P_1(T)$, $P_2(T)$, and $P_3(T)$ are applied at $X = L/4$, $L/2$, and $3L/4$, respectively. The coefficient of external damping is denoted C.

Consider the nondimensional quantities

$$x = X/L \qquad y = Y/(2r) \qquad y_0 = Y_0/(2r)$$
$$\lambda = \Lambda/(2r) \qquad t = T\sqrt{EI/(\mu L^4)} \qquad c = CL^2/\sqrt{EI\mu}$$
$$p_k = P_k L^3/(2\pi^4 EIr) \qquad k = 1,2,3 \tag{2}$$

and let the downward deflection be denoted by w, i.e.,

$$w(x,t) = y_0(x) - y(x,t) \tag{3}$$

The equation of motion under the standard shallow-arch assumptions is[1]

$$\frac{\partial^2 w}{\partial t^2} + c\frac{\partial w}{\partial t} + \frac{\partial^4 w}{\partial x^4} + m\frac{\partial^2 (w - y_0)}{\partial x^2} = \pi^4 \sum_{k=1}^{3} p_k \delta[x - (k/4)] \tag{4}$$

Received Oct. 9, 1981; revision received Feb. 17, 1982.

*Graduate Student, Department of Civil Engineering, presently with Exxon Research and Engineering Co., Florham Park, N.J.

†Professor, Department of Civil Engineering.

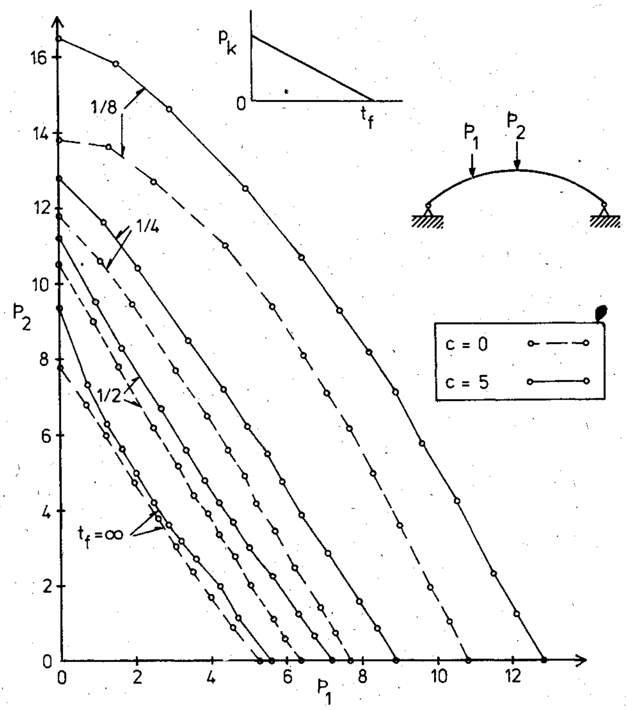

Fig. 1 Interaction curves when $p_3 = 0$.

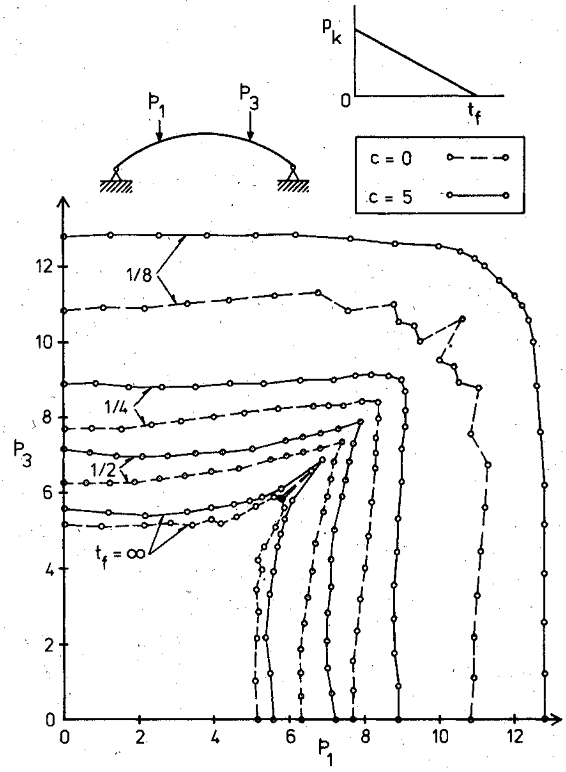

Fig. 2 Interaction curves when $p_2 = 0$.

where δ is the Dirac delta function and

$$m = 2\int_0^1 \frac{\partial w}{\partial x}\left[2\frac{\mathrm{d}y_0}{\mathrm{d}x} - \frac{\partial w}{\partial x}\right]\mathrm{d}x \tag{5}$$

The boundary conditions are

$$w = 0, \qquad \frac{\partial^2 w}{\partial x^2} = 0 \text{ at } x = 0, 1 \tag{6}$$

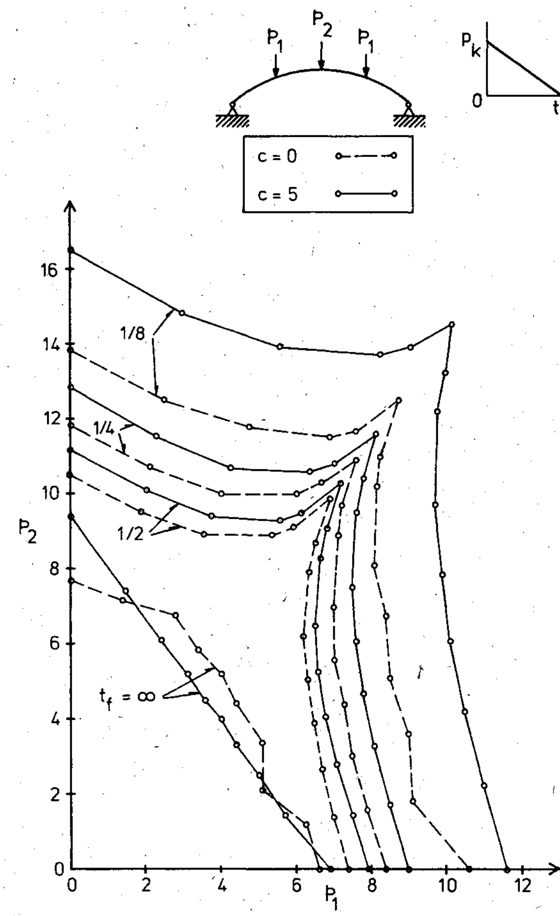

Fig. 3 Interaction curves when $p_1 = p_3$.

The pulse loads are assumed to rise instantaneously to the values p_k at $t = 0$ and then to decrease linearly to zero at $t = t_f$. Step loads are a special case of such right triangular pulse loads with $t_f \to \infty$,[8] whereas impulse loads correspond to $t_f \to 0$.

Numerical results are obtained by assuming

$$w(x,t) = \sum_{i=1}^{N} q_i(t)\sin i\pi x \tag{7}$$

and applying Galerkin's method. The resulting N nonlinear, ordinary differential equations in $q_i(t)$ are integrated by a finite difference procedure, and critical loads are determined by the Budiansky-Roth criterion[9] corresponding to a sudden jump in the maximum response.[7] It was found that $N = 5$ was sufficient to give accurate results.

Interaction Curves

Interaction curves are presented in Figs. 1-3 for the arch rise parameter value $\lambda = 5$, pulse lengths $t_f = 1/8$, $1/4$, $1/2$, and ∞ (step loads), and damping coefficients $c = 0$ (undamped) and $c = 5$. Undamped cases are depicted with dashed lines. The lowest natural period of the arch is $1/(2\pi)$,[10] and the case $c = 5$ corresponds to 3.6% of critical damping in the first mode ($i = 1$) of Eq. (7). The results for step loads with no damping are taken from Ref. 7.

Computed values of critical load combinations are represented by circles. In Fig. 1 results are obtained by setting $p_3 = 0$, fixing the ratio p_1/p_2, and increasing the magnitudes of the loads until snap-through occurs (i.e., using proportional loading along a ray in the plane of p_1 vs p_2). By symmetry, p_1 and p_3 could be interchanged. The case of no central load ($p_2 = 0$) is depicted in Fig. 2 and the interaction curves are symmetric about the ray $p_1 = p_3$. Finally, symmetric load distributions are considered in Fig. 3 where p_1 and p_3 are equal to each other and their ratio with p_2 is varied.

As one might expect, the interaction curves move closer to the origin with increasing pulse duration t_f. In other words, the critical value of the initial load magnitude at $t=0$ decreases if the load is applied to the arch for a longer time. Step loading provides the limiting case. (If one were to use the pulse areas $p_k t_f/2$ as the coordinates on the axes, the interaction curves would move inward with decreasing pulse duration and would approach the curve for impulse loads.) The presence of damping is seen to increase the critical loads, except in the case of step loading in Fig. 3, and to cause little change in the shapes of the curves, except in the aforementioned case and for $t_f = 1/8$ in Fig. 2 near the ray $p_1 = p_3$.

The lowest critical load, as far as the sum of the magnitudes is concerned, occurs when either p_1 or p_3 is applied by itself. The arch is especially resistant to snap-through when the loading is symmetric. At $p_1 = p_3$ in Fig. 2, the interaction curves develop a spike as $t_f \to 0$, indicating extreme sensitivity to asymmetric imperfections.

Knowledge of the shapes of interaction curves can sometimes be used to obtain bounds and approximations for critical load combinations in related problems. In most of the results presented here, for example, a straight line connecting the critical loads on the two axes furnishes stable load combinations (although they are sometimes less than one-half of the critical values). The shapes of the interaction curves may change as the pulse duration changes, and no general convexity property can be stated.

Acknowledgment

This research was supported by the National Science Foundation under Grant CME-7920781.

References

[1] Humphreys, J.S., "On Dynamic Snap Buckling of Shallow Arches," *AIAA Journal*, Vol. 4, May 1966, pp. 878-886.

[2] Fulton, R.E. and Barton, F.W., "Dynamic Buckling of Shallow Arches," *Journal of the Engineering Mechanics Division*, ASCE, Vol. 97, No. EM3, June 1971, pp. 865-877.

[3] Lock, M.H., "Snapping of a Shallow Sinusoidal Arch Under a Step Pressure Load," *AIAA Journal*, Vol. 4, July 1966, pp. 1249-1256.

[4] Hegemier, G.A. and Tzung, F., "Influence of Damping on the Snapping of a Shallow Arch Under a Step Pressure Load," *AIAA Journal*, Vol. 7, Aug. 1969, pp. 1494-1499.

[5] Huang, N.C. and Nachbar, W., "Dynamic Snap-Through of Imperfect Viscoelastic Shallow Arches," *Journal of Applied Mechanics*, Vol. 35, No. 2, June 1968, pp. 289-296.

[6] Johnson, E.R., "The Effect of Damping on Dynamic Snap-Through," *Journal of Applied Mechanics*, Vol. 47, No. 3, Sept. 1980, pp. 601-606.

[7] Gregory, W.E. Jr. and Plaut, R.H., "Dynamic Stability Boundaries for Shallow Arches," *Journal of the Engineering Mechanics Division*, ASCE, in press.

[8] Kao, R. and Perrone, N., "Dynamic Buckling of Axisymmetric Spherical Caps with Initial Imperfections," *Computers and Structures*, Vol. 9, No. 5, Nov. 1978, pp. 463-473.

[9] Budiansky, B. and Roth, R.S., "Axisymmetric Dynamic Buckling of Clamped Shallow Spherical Shells," NASA TN D-1510, Dec. 1962, pp. 597-606.

[10] Plaut, R.H. and Johnson, E.R., "The Effects of Initial Thrust and Elastic Foundation on the Vibration Frequencies of a Shallow Arch," *Journal of Sound and Vibration*, Vol. 78, No. 4, Oct. 1981, pp. 565-571.

Application of Variational Embedding Technique to Nonlinear Heat Transfer Problems

Yih-Min Chang,* Cha'o-Kuang Chen,† and Cheng-I Weng†
National Cheng Kung University
Taiwan, Republic of China

Introduction

It is sometimes necessary to include nonlinear boundary conditions and material property variations into the analysis of a heat conduction problem.[1-5] Because these effects cannot be taken into account by using classical methods, approximate methods including these effects in a systematic manner are needed. Two such methods are the heat balance integral technique and the variational technique.

In this Note, the variational embedding technique is presented to be a new approximate method which can also include these aforesaid effects in a systematic manner. The theory of variational embedding was systematically developed by Edelem.[6] Bhatkar and Rao have applied it to the distributed systems control.[7] Now, this technique is used to solve the radiative heat transfer problem of a semi-infinite body with variable thermal properties. The results for several examples are shown in graphical form and comparisons are made with other available solutions.

Methods and Results

Consider the heat loss from a semi-infinite solid at a rate proportional to a power m of the surface temperature when both thermal conductivity and heat capacity are a function of temperature. Its initial temperature is T_0 while the ambient temperature is T_e. The governing partial differential equation for the problem can be written in the form:

$$u(T)\frac{\partial T}{\partial t} = \frac{\partial}{\partial x}\left[k(T)\frac{\partial T}{\partial x}\right] \tag{1}$$

subject to the following conditions

$$T(x,0) = T_0 \tag{2}$$

$$k\frac{\partial T}{\partial x}\bigg|_{x=0} = h[T^m(0,t) - T_e^m] \tag{3}$$

The thermal conductivity and heat capacity are assumed to be a power series of temperature

$$k(T) = k_R\left[1 + \sum_{j=1}^{\infty} a_j (T/T_0)^j\right] \tag{4}$$

$$u(T) = u_R\left[1 + \sum_{j=1}^{\infty} b_j (T/T_0)^j\right] \tag{5}$$

Received Oct. 9, 1981; revision received June 11, 1982.

*Researcher, Department of Mechanical Engineering.
†Professor, Department of Mechanical Engineering.